SERI/TP-257-3695
UC Category: 261
DE90000327

Aerodynamic Pressure Measurements on a Rotating Wind Turbine Blade

C. P. Butterfield
M. D. Jenks
D. A. Simms
W. P. Musial

May 1990

Prepared for the 36th Instrument Society of America
International Instrumentation Symposium
Denver, Colorado
7-10 May 1990

Prepared under Task No. WE011001

Solar Energy Research Institute
A Division of Midwest Research Institute

1617 Cole Boulevard
Golden, Colorado 80401-3393

Prepared for the
U.S. Department of Energy
Contract No. DE-AC02-83CH10093

NOTICE

Printed in the United States of America
Available from:
National Technical Information Service
U.S. Department of Commerce
5285 Port Royal Road
Springfield, VA 22161

Price: Microfiche A01
Printed Copy A03

Codes are used for pricing all publications. The code is determined by the number of pages in the publication. Information pertaining to the pricing codes can be found in the current issue of the following publications which are generally available in most libraries: *Energy Research Abstracts (ERA)*; *Government Reports Announcements* and Index (*GRA* and I); *Scientific and Technical Abstract Reports (STAR)*; and publication NTIS-PR-360 available from NTIS at the above address.

Aerodynamic Pressure Measurements on a Rotating Wind Turbine Blade

C. P. Butterfield
M. Jenks
D. A. Simms
W. Musial

Solar Energy Research Institute
1617 Cole Boulevard
Golden, Colorado 80401

ABSTRACT

Wind turbine generators commonly operate in either a fixed-pitch or variable-pitch mode. In variable-pitch mode the angle of the blade is changed as the wind speed varies to maintain near optimum airfoil angle of attack and to regulate peak power. The more common fixed-pitch rotors do not change pitch angle to regulate peak power. Instead the blade is allowed to stall aerodynamically. This approach results in rapid relief of loads caused by gusts and is more reliable and cost effective. However, the designer must accurately understand the rotating-blade stall behavior of the airfoil in order to predict turbine loads. To understand such stall behavior a test program that uses specially designed instrumentation has been conducted by the Solar Energy Research Institute (SERI).

A microprocessor-controlled measurement system has been designed and built to make accurate measurements of low pressures on a rotating wind turbine blade. This Pressure System Controller (PSC) is capable of simultaneously operating four pressure scanners (128 channels total) while rotating on a wind turbine blade. Calibrations and purge sequences are performed automatically on all 128 channels while the turbine is rotating. Data are fed to a Pulse Code Modulation (PCM) data-acquisition system and recorded on magnetic tape for later processing. Accurate measurements have been made down to pressures of 11 microbars (0.00018 psi) for low Reynolds Number tests. These rotating-blade pressure measurements are used to compare with wind tunnel data to see how blade rotation alters airfoil performance.

A description of the test setup and instrumentation design is given along with example results. Recommendations for future work and changes in the design approach are also discussed.

INTRODUCTION

Most wind turbines experience aerodynamic stall during normal operating conditions over small and sometimes large areas of the blade. The majority of horizontal-axis wind turbines (HAWT) use stall to regulate peak power and loads. The operation of airfoils in stall and beyond stall has led to several problems. First, very few wind tunnel data exist for airfoil performance beyond maximum lift coefficient (C_{Lmax}). Because wind turbines commonly operate at very high angles of attack (20 - 40 degrees) this leads to guessing the airfoil performance between 12 and 30 degrees. Beyond 30 degrees, flat plate theory has been used by most designers. Basing performance and loads predictions on this uncertain airfoil performance data contributes to significant errors in peak performance estimates.

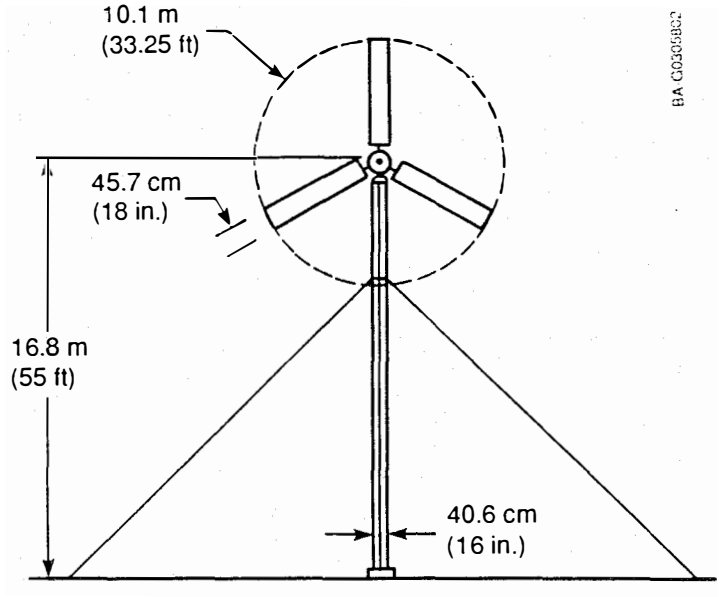

Induction generator rating	20 kW
Induction generator speed range	1800-1860 rpm
Gearbox ratio	25.1:1
Rotor speed	74.1 rpm
Rotor diameter	33.25 ft
Rotor solidity	0.0615
Blade chord	1.5 ft
Power coefficient, Max ($C_{P\ MAX}$)	0.38°
Tip speed ratio at $C_{P\ MAX}$	5.25°
Wind speed at $C_{P\ MAX}$	17.0 mph
System efficiency at $C_{P\ MAX}$	83%
Output power at VW = 24 mph	15 kW*
Rotor coning angle	3-1/2°
Razor/Nacelle assembly wt.	2,589 lb.
Drive axis height	55 ft
Tower section	16.0 in./0 dia, 3/8 in. wall
Guy base	80 ft

*Predicted

Figure 1. Characteristics of the Combined Experiment Wind Turbine

Second, stall performance of an airfoil used on a rotating wing such as a HAWT appears to be modified by three-dimensional flow effects. It is common for wind turbine designers to underestimate peak performance and loads. Part of the cause is poor airfoil data as mentioned above, but there is an additional effect caused by rotation of the blade. The lift curve slope and C_{Lmax} appear to be reduced on outboard blade sections, and inboard C_{Lmax} appears to be increased, according to Madsen (1). In order to understand the physics controlling this phenomenon, detailed airfoil performance measurements must be studied on a rotating wing.

Because stall is such an important issue for predicting both steady and unsteady loads, SERI, sponsored by the United States Department of Energy, has begun a detailed measurement program on a 10-meter 3-bladed HAWT. This test has produced measurements of (1) far-field atmospheric boundary layer, (2) near-field inflow using a vertical plane array and high-frequency-response anemometry, (3) airfoil pressure distributions at 80% radius, (4) video images of surface flow patterns, (5) blade loads at nine spanwise locations, and (6) turbine loads.

This detailed data set is being used to understand how turbulent inflow affects unsteady aerodynamics, fatigue loads, and yawed operation loads. This paper will focus only on rotating-wing aerodynamic pressure measurements and the instrumentation that was developed in support of that effort.

TEST SETUP

As mentioned earlier, the test program used a 10-meter-diameter three-bladed down-wind turbine with pitch control (Figure 1). A constant 45-cm chord blade was used with an S809 airfoil, which is described by Tangler (2). The details of the overall test setup are covered by Butterfield (3). The discussion in this paper will address only the details of the pressure measuring system and the flow angle sensor.

Figure 2 describes how the pressure transducers and pressure taps are installed in the HAWT blade. Signals and transducer

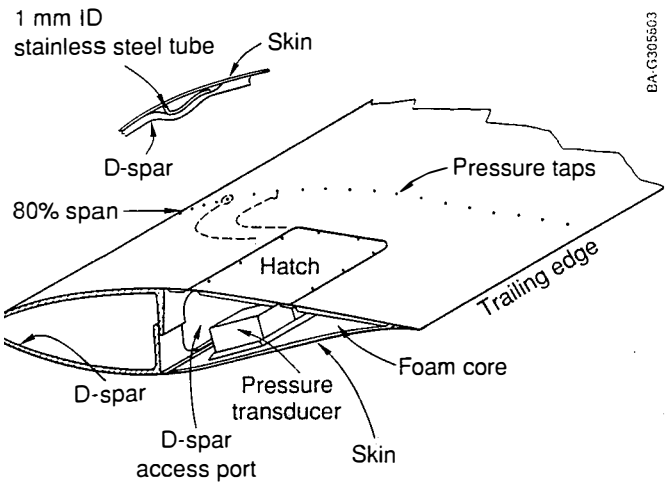

Figure 2. Transducer Installation in Blade

controls are transmitted down the blade to the hub via cables and tubes laminated into the blade skin.

FLOW-ANGLE SENSOR

Because the main objective of these aerodynamic measurements was to compare wind tunnel data with rotating-blade data, an accurate means of comparison was very important. The most direct and common measurement for comparing various data sets is "angle of attack." This is a fairly easy measurement to make in the wind tunnel; but on the rotor this is not the case. Local upwash effects, as well as induced velocities created by rotor wake expansions, distort the flow. Figure 3 shows typical streamlines under the influence of circulation-induced upwash. It was decided to use both analytical and experimental techniques in a "best-effort" approach to accurately determine the correct angle of attack from measured local flow angles (LFAs). The analytical approach was used to confirm the experimental corrections as described later in this paper.

Figure 4 shows the flow-angle sensor (FAS) developed by SERI for this test program.

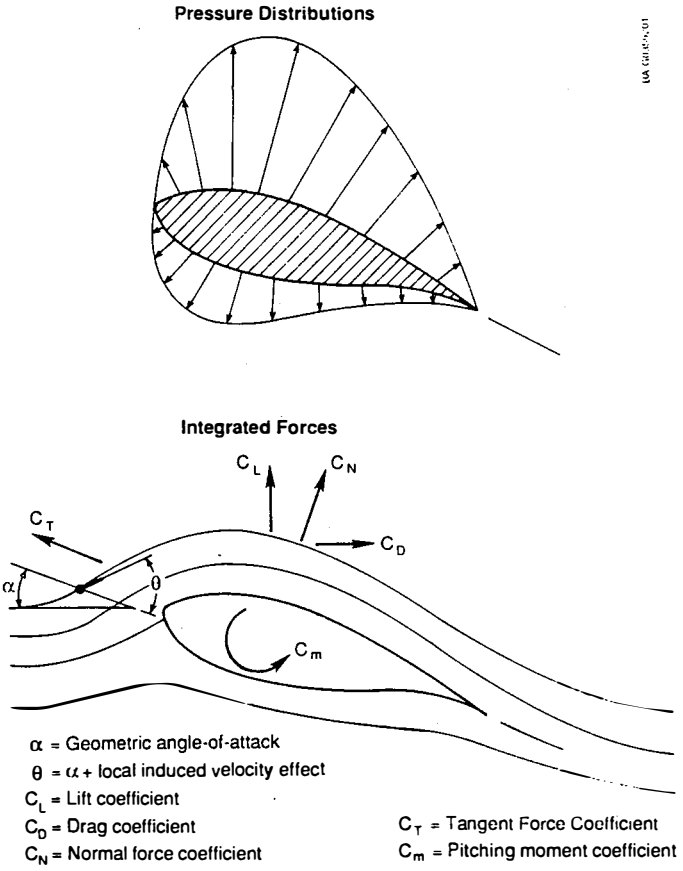

Figure 3. Upwash Effect and Terminology

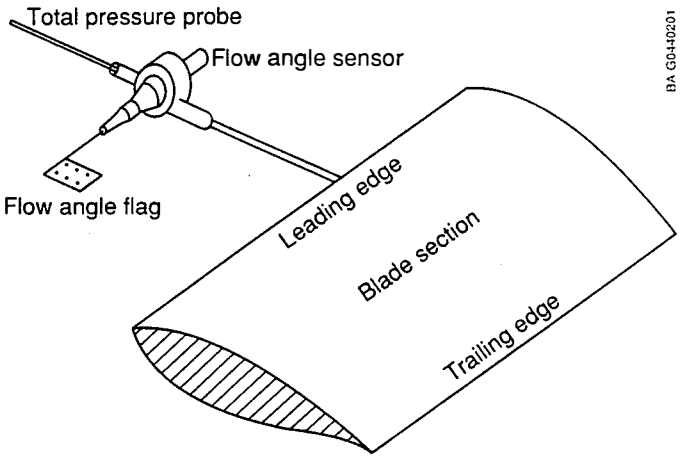

Figure 4. Local Flow-Angle Transducer

Lenschow (4) describes early development and testing of a similar sensor that was used in atmospheric flight testing. The sensor uses a very lightweight ridged flag which aligns itself with the local flow. The flag angle is measured with a commercial rotary position sensor. The analog signal generated is recorded with the data-acquisition system. Flag angles can be measured within 0.1 degree of accuracy. The sensor is mounted 0.8 chord lengths ahead of the leading edge on the 45.7-cm-chord blade. It was positioned at 86% of blade span (6% outboard of pressure taps) in order to limit flow disturbances on the blade near the pressure taps. A total pressure probe was mounted at the tip of the sensor to record dynamic pressure measurements.

The accuracy of flow-angle measurements and the relationship to the wind tunnel angle of attack were issues of concern. To investigate these issues the sensor and probe were mounted on the wind tunnel model during tunnel testing. The effects of upwash, frequency response, and Reynolds Number were determined.

Figure 5 shows the results of steady tests. The dashed line in Figure 5 indicates a zero correction line or a condition in which the flow-angle sensor would measure the same angle as the geometric model angle during the wind tunnel testing. Triangles show data measured by the FAS with a solid-line curve fit to these data. As can be seen, the upwash effect is important. At a geometric angle of 10 degrees the FAS indicates a 14-degree angle. The 4-degree discrepancy is caused by the net effect of bound circulation and wake-induced flow. The solid line shows a prediction of upwash effect. The Kutta-Joukowski Theorem was used to estimate the bound circulation, and the Biot-Savart Law was used to determine the local induced velocity. The induced-velocity vector was added to the resultant inflow-velocity vector to determine the corrected flow angle. The correlation is strong at low angles where the flow is attached to the airfoil, but as the

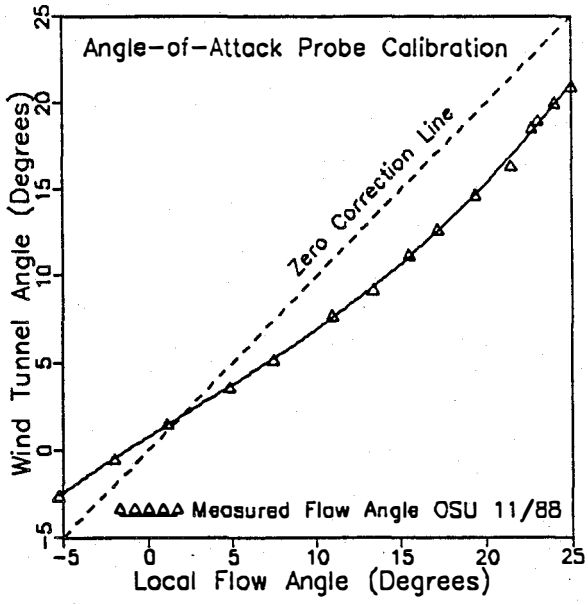

Figure 5. Wind Tunnel Calibration of the Local Flow-Angle Sensor

angle increases and the flow separates the correlation weakens. Reynolds Number effects were estimated to be insignificant for the steady-state wind tunnel tests. The wind tunnel data correction was used as the steady correction in field test data analysis.

To test the dynamic response of the FAS, the flag was deflected and released while the tunnel was running at various Reynolds Numbers. The ringdown was recorded, from which a second-order-system natural frequency and logarithmic-damping ratio was determined. Figure 6 shows the results of a ringdown at Reynolds Number = 1,000,000 along with the analytical approximations. From the comparisons it is clear that the FAS is well damped but not critically damped. Also, a second-order differential equation models the response well. The model shown plus the Inverse Transfer Function technique described by Irwin (5) will be used in future data analyses to correct the frequency response, in both phase and magnitude, out to about 15 Hz.

This discussion addresses the issue of FAS dynamic characteristics. However, dynamic

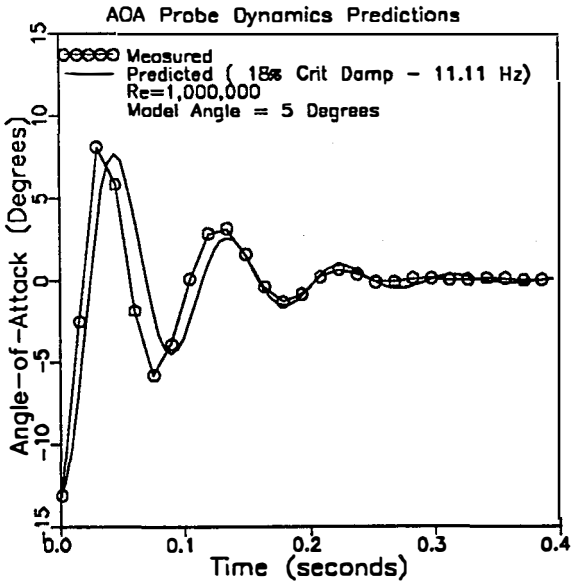

Figure 6. Dynamic Response Test of the Flow-Angle Sensor (Reynolds Number = 10^6)

bound circulation changes could cause local flow-field modifications that would alter the steady correction shown in Figure 4. These effects are unknown at this time. Future dynamic stall wind tunnel tests will attempt to address this issue. The reader should note that LFA data presented throughout this report are not corrected for either FAS dynamic characteristics or dynamic flow-field effects.

PRESSURE MEASUREMENT SYSTEM

This test program required that pressure measurements be made to within 2-3% of the local dynamic pressure and have a bandwidth of 100 Hz. At the 80% blade span this equates to an accuracy of 137 microbars (0.002 psi); at the inboard blade station this equates to 11 microbars (0.0002 psi). To obtain this accuracy we determined it necessary to be able to conduct frequent range and zero calibrations during the test. This would minimize systematic errors and help the test engineer track errors caused by

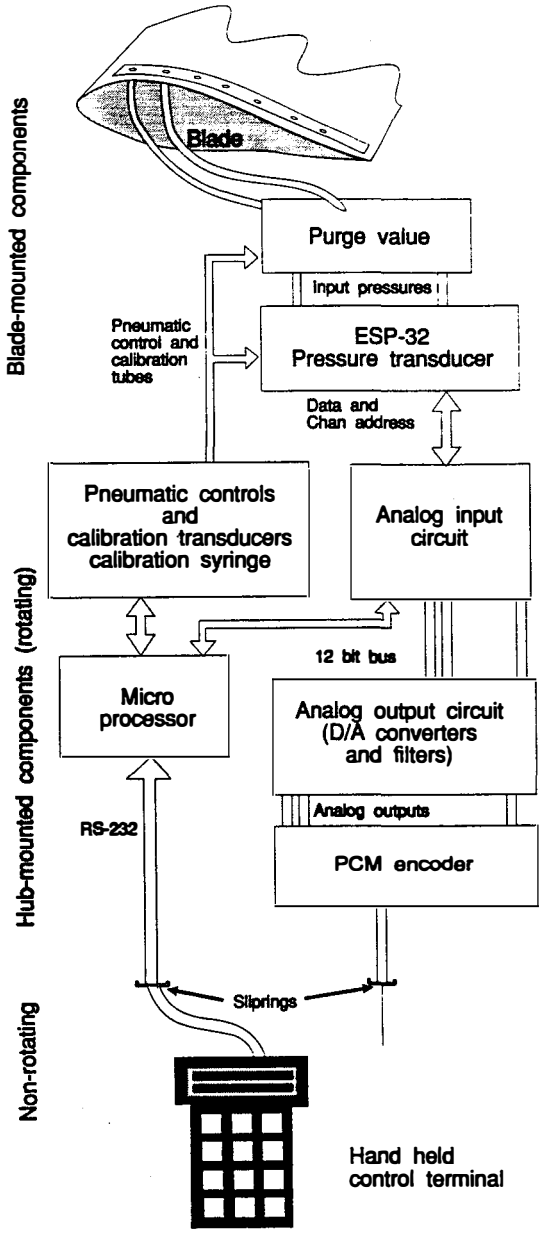

Figure 7. Pressure System Controller Block Diagram

drift. For this reason a scanner-type transducer was used (ESP-32 made by Pressure Systems International) that had remote calibration capability. The transducer was installed in the blade as close to the surface pressure-tap locations as possible.

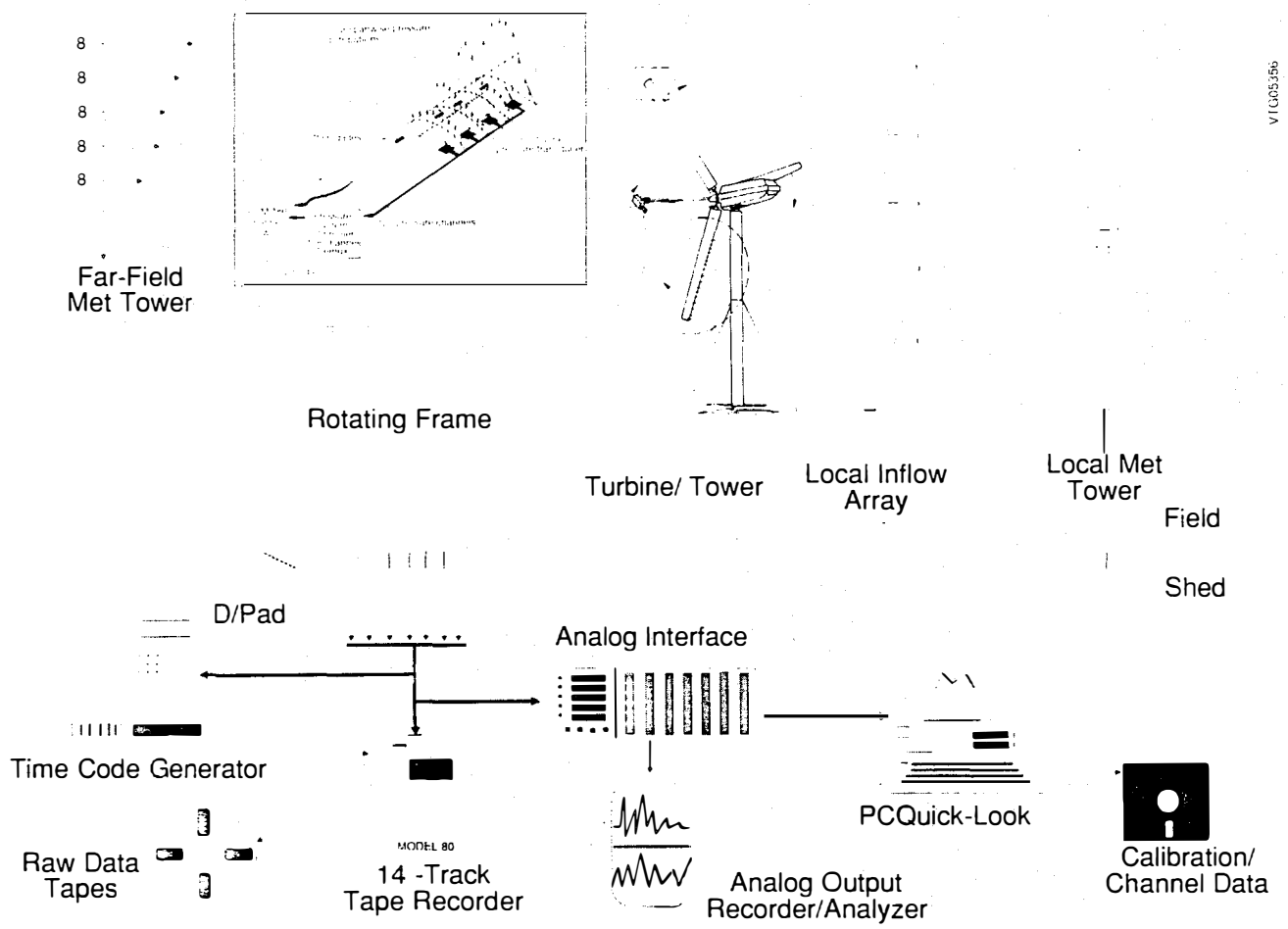

Figure 8. Combined Experiment PCM Streams

Remote control of calibration, scanner addressing, and signal demultiplexing of the analog multiplexed signal were performed by a microprocessor controller mounted on the wind turbine hub. One of the major requirements was that the control system rotate with the wind turbine hub while conducting the stated functions. This allowed calibration signals to be recorded during rotating conditions. This procedure was important in accounting for effects of centrifugal force. Figure 7 shows a block diagram of the pressure system controller (PSC) that SERI designed for this purpose.

The range calibration sequence is started by energizing a pneumatic valve in the controller. Pneumatic pressure shuttles a plate in a Purge Valve, which (1) connects all pressure input ports to a common calibration pressure line and (2) connects all surface pressure-tap tubes to a common purge pressure line. Calibration pressure is applied by a motorized syringe under microprocessor control. Calibration pressure is measured by a Setra 237 differential pressure transducer mounted in the PSC. Simultaneously, purge pressure is applied to the pressure-tap tubes. The syringe provides

a means of accurately controlling small positive and negative pressures without any external pressure source. The PSC only requires a 0.094-cubic-meter (1-cubic-foot) dry nitrogen-control pressure source.

Zero calibration is accomplished by energizing a second valve, which again shuttles a plate in the ESP-32 transducer, connecting all input pressures to the reference pressure. This standard feature of the transducer is used every five minutes of testing to record zero calibrations on all channels.

A frequency response of 100 Hz is required to study dynamic stall behavior on the rotating wind turbine blade. To accomplish this the pressure port address is incremented from port to port at 16,646 Hz, resulting in complete scans of all 32 ports at 520 Hz and a port-to-port settling time of 60 microseconds. Samples are then passed on to the PSC as an analog multiplexed signal, digitized, distributed to 32 D/A converters on a digital bus, and passed through individual reconstruction filters. The filters are 100-Hz-precision four-pole Butterworth filters. The 32 reconstructed analog output signals are then passed to the PCM system. The output of the PCM system is passed over sliprings to the control building and recorded on a wide-band tape recorder for later processing. Figure 8 describes the overall data-acquisition system for the test program.

A natural question would be, "Why convert to digital in the PSC, then back to analog outputs, only to convert once again into digital in the PCM system?" When the system was designed a frequency multiplexing system was to be used for data recording. This system would have required analog outputs. Although the processing appears cumbersome, it does provide flexibility and it has been very stable.

The PSC was designed to control and process data from four ESP-32 transducers in parallel. As many as 128 pressure channels can be processed simultaneously without any loss in performance.

Pressure-tap tube acoustical frequency response usually limits accurate pressure measurements to 20% of the first harmonic frequency. In the case of a 45-cm- (18-in.)-long tube, the first harmonic is approximately 80 Hz according to Irwin (5). Irwin describes how this can be corrected in software by first measuring the acoustical transfer function of the tube and then applying the measured transfer function to the data in the frequency domain. A recursive filter can also be used to apply the transfer function to the data in the time domain. This technique is used to get full 100-Hz bandwidth from the pressure signals.

The reference pressure for each transducer is an important and difficult issue for transducers located in a rotating environment. Centrifugal forces act on the air in the tube and change the pressure throughout the radius of the wind turbine rotor. If the tube is terminated inside the blade, it is exposed to uncertain pressure gradients inside the blade. It was decided to lead the reference tubes from each transducer to the hub. The reference pressure at the transducer was calculated by using the following equation.

$$P_{atm} + P_{cf} = 1/2 \text{ (air density)}(r * \text{omega})^2$$

Where: P_{atm} = atmospheric pressure
P_{cf} = pressure caused by centrifugal force
r = radial distance to transducer
omega = rotor speed

Tests have been run to verify the accuracy of the equation and have confirmed the predicted values to within the measurement accuracy of the transducer.

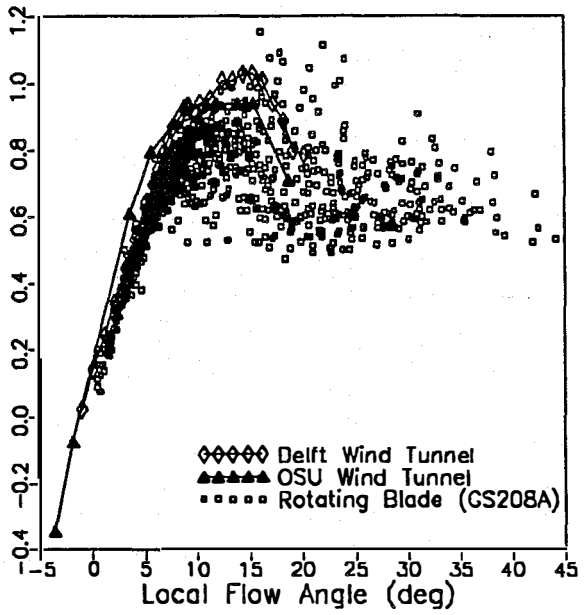

Figure 9. Lift Characteristics at Deep Stall

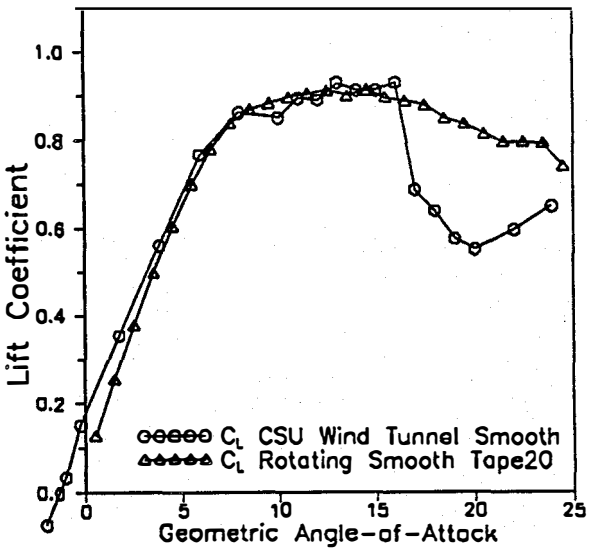

Figure 10. Wind Tunnel and Rotating C_l Comparisons

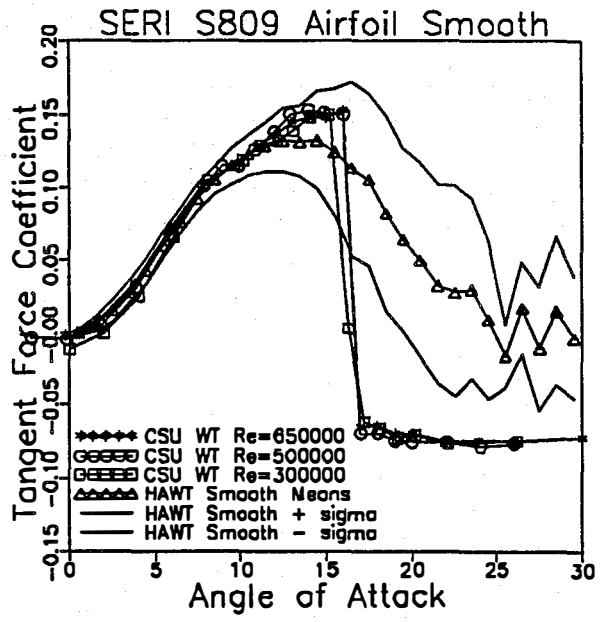

Figure 11. Tangent Force Comparisons

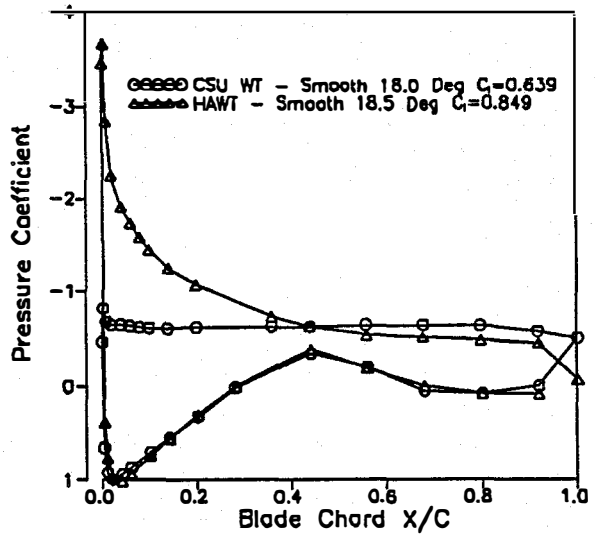

Figure 12. Pressure Distribution Comparisons

SAMPLE RESULTS

Figure 9 compares wind tunnel lift coefficient data and data measured on the HAWT rotor. Pressure distributions were integrated to get normal and chordwise (tangent to chord line) force coefficients. These data were converted to lift and pressure drag and were block averaged from 522-Hz to 10-Hz sample rate. The correlation is relatively good with low scatter for corrected local flow angles less than 8 degrees. Beyond this angle, stall begins to dominate the airfoil behavior, causing significant scatter. Butterfield (6) suggest that much of the scatter shown is caused by stall hysteresis and other dynamic effects.

Figure 10 shows the same data averaged using the method of bins. From this curve the differences between wind tunnel and rotating-blade stall behavior are clearer. Stall in the wind tunnel is abrupt at 17 degrees; in the rotating environment it occurs far more gradually. Figure 11 shows even more dramatic differences when comparing tangent coefficients. On the HAWT rotor, tangent forces remain significantly positive long after the normal stall angle. Since tangent forces provide most of the torque for HAWT rotors, higher than predicted power levels would be expected. In fact Madsen (1) and others have reported this very common behavior for stall-controlled wind turbines.

The cause of this delayed stall is shown in Figure 12, where pressure distributions are compared for 18 degrees. It is clear that a leading suction peak is present in the HAWT data where the wind tunnel data show no peak. This implies that flow around the leading edge remains attached for the rotating blade, long after leading separation on the wind tunnel airfoil. Figure 13 shows pressure distributions up to 25 degrees LFA, and suction peaks can be seen on even the highest-angle curve. Musial (7) describes how delayed stall is actually more significant when severe leading-edge roughness is applied.

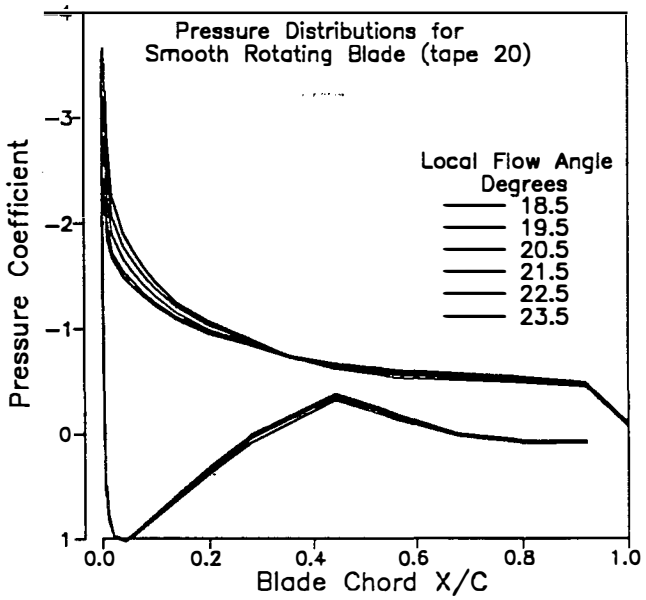

Figure 13. Pressure Distributions at High LFAs.

The cause of delayed stall is not yet known. Spanwise pressure gradients, which exist on HAWT blades, could modify boundary layer profiles and hence delay separation. Research is being conducted at SERI to determine the basic fluid mechanics of the rotating-blade boundary layer. This research will lead to better prediction of performance and loads. It may also lead to optimal airfoil designs for wind turbines.

RECOMMENDATIONS AND CONCLUSIONS

SERI has used an ESP-32 scanner in a rotating wind turbine blade with great success. Frequent remote calibrations have been instrumental in maintaining accuracy limits. If the system were designed again, a PCM encoder should be designed directly into the PSC to avoid the need for reconversion to analog signals. However, the analog system used was stable.

ACKNOWLEDGMENTS

Many people have contributed to this research program. Bob Thresher, Al Eggers, Craig Hansen, Bob Akins, George Scott, and Karl Danninger all have made direct contributions deserving recognition and thanks. This work was conducted under U.S. Department of Energy contract AC02-83CH10093. Without the support of the DOE the program would not have been possible.

REFERENCES

1. Madsen, H. A., F. Rasmussen, and T. F. Pedersen, "Aerodynamics of a Full-Scale HAWT Blade," presented at European Community Wind Energy Conference, 1988.

2. Tangler, J. L., "Status of the Special-Purpose Airfoil Families," presented at American Wind Energy Association Windpower '87, San Francisco, California.

3. Butterfield, C. P., "Aerodynamic Pressure and Flow-Visualization Measurements from a Rotating Wind Turbine Blade," presented at the Eighth ASME Wind Energy Symposium, Houston, Texas, January 1989.

4. Lenschow, D. H., "Vanes for Sensing Incidence Angles of the Air from an Aircraft," Journal of Applied Meteorology, Vol. 10, No. 6, 1971, pp. 1339-1343.

5. Irwin, H.P.H.H., K. R. Cooper, and R. Hirard, "Correction of Distortion Effects Caused by Tubing Systems in Measurements of Fluctuating Pressures," Journal of Industrial Aerodynamics, Vol. 5, 1979, pp. 93-107.

6. Butterfield, C. P., "Three-Dimensional Airfoil Performance Measurements on a Rotating Wing," presented at European Wind Energy Conference, July 1989.

7. Musial, W., C. P. Butterfield, and M. Jenks, "Three-Dimensional Roughness Effects on a HAWT Blade," presented at Ninth ASME Wind Energy Symposium, New Orleans, Louisiana, January 1990.